Supporting Information

Hierarchical Fermat Helix-structured Electrochemical Sensing Fibers Enable Sweat Capture and Multi-biomarker Monitoring

Hang Tian, Lichao Wang, Weifeng Yang, Kerui Li, Qinghong Zhang, Yaogang Li,*
Hongzhi Wang, Chengyi Hou*

List of Contents

Figure S1. SEM image of the fiber electrode with 3D folded graphene structure at different magnifications.

Figure S2. Characterization of successful graphene deposition.

Figure S3. SEM image of CNT sensing fiber structures

Figure S4. Digital photograph of Fermat helical structure-based electrochemical sensing fibers.

Figure S5. Response of graphene with different cyclic deposition amounts in redox probe solutions($[Fe(CN)_6]^{3-/4-}$ and KCl solution).

Figure S6. Current curves (i-t) of CNT and rGO-CNT in the same concentration of glucose solution.

Figure S7. Observation of the ink absorption process on the fiber by optical microscopy.

Figure S8. Resistance change of CNT and HFH-ESF after 6000 times of 90 degree bending.

Figure S9. Fluorescent images of live dead cells after 24 hours of cell viability testing in HFH-ESF cultures.

Figure S10. The interference study for individual (a) glucose, (b) lactate, (c) K^+, (d) Na^+, (e) Ca^{2+}, and (f) pH-sensing fibers

Figure S11. The reproducibility of (a) glucose, (b) lactate, (c) K^+, (d) Na^+, (e) Ca^{2+}, and (f) pH-sensing fibers.

Figure S12. The long-term stability of the (a) glucose, (b) lactate, (c) K^+, (d) Na^+, (e) Ca^{2+}, and (f) pH-sensing fibers.

Figure S13. The processing and structure of textile.

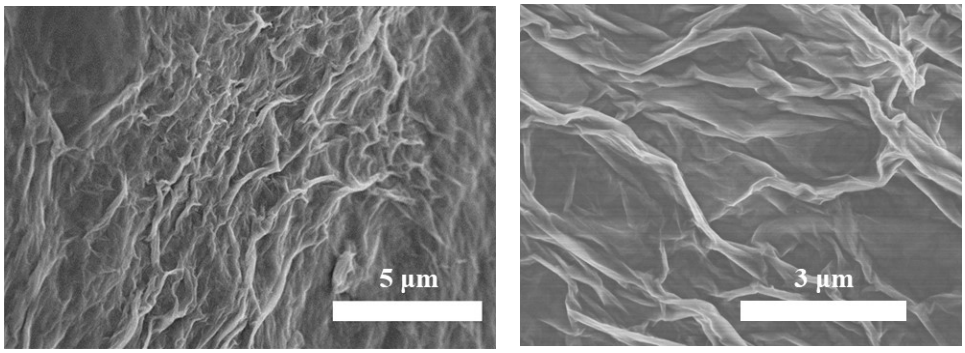

Figure S1. SEM image of the fiber electrode with 3D folded graphene structure at different magnifications.

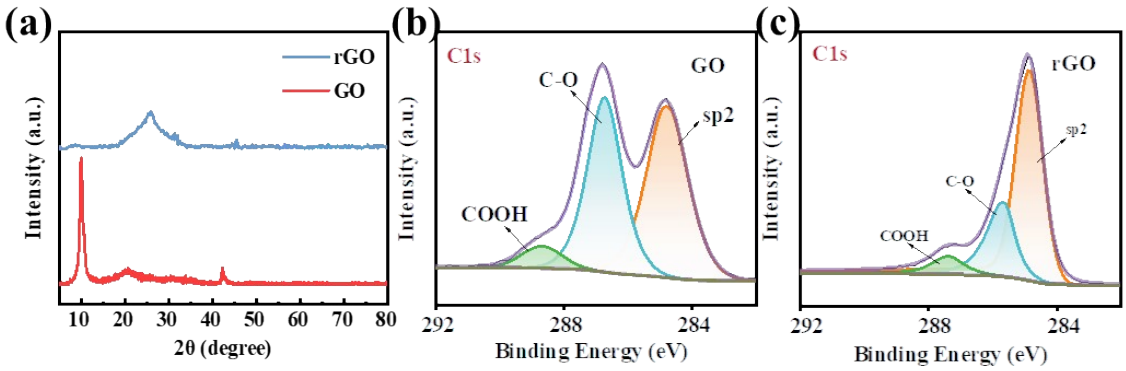

Figure S2. (a) XRD images of graphene oxide and graphene. C1s XPS spectra of (b) graphene oxide, and (c) graphene network electrode, confirming the successful reduction of graphene oxide.

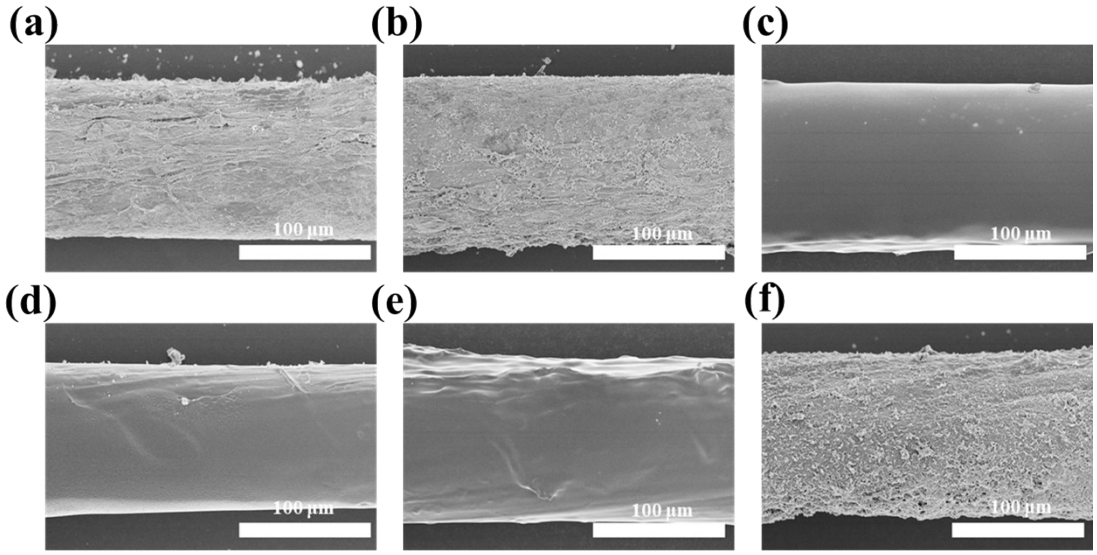

Figure S3. SEM image of CNT fiber sensing structures with (a) glucose, (b) lactate, (c) K^+, (d) Na^+, (e) Ca^{2+}, and (f) pH.

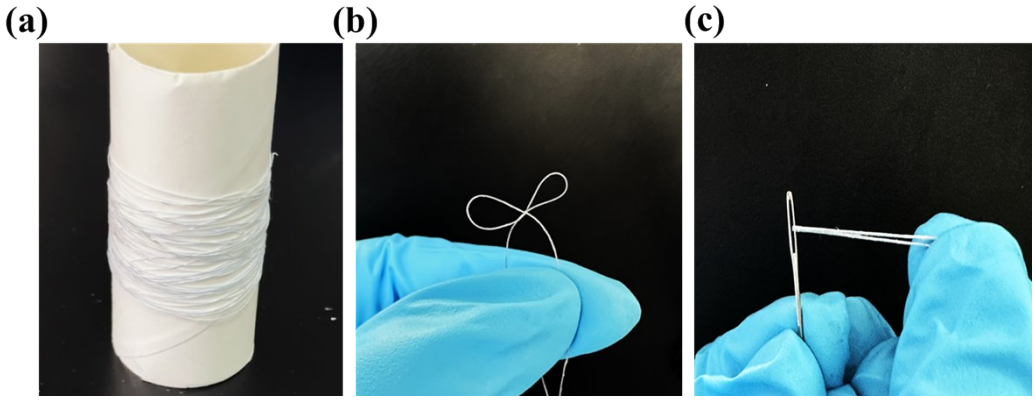

Figure S4. (a) Digital photograph of a roll of Fermat helical structure-based electrochemical sensing fibers. (b) Digital photograph of the fiber electronics woven into a butterfly knot. (c) Digital photograph of the fiber electronics threaded through a needle.

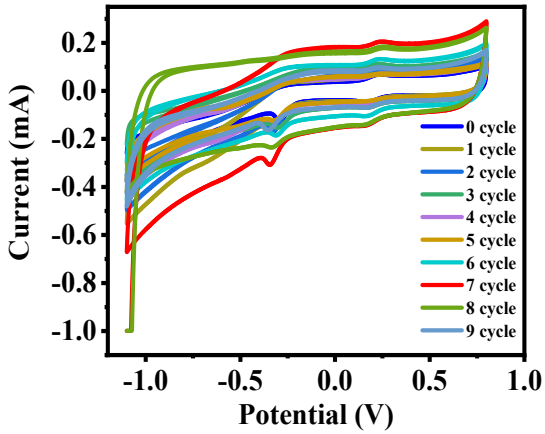

Figure S5. Response of graphene with different cyclic deposition amounts in redox probe solutions($[Fe(CN)_6]^{3-/4-}$ and KCl solution).

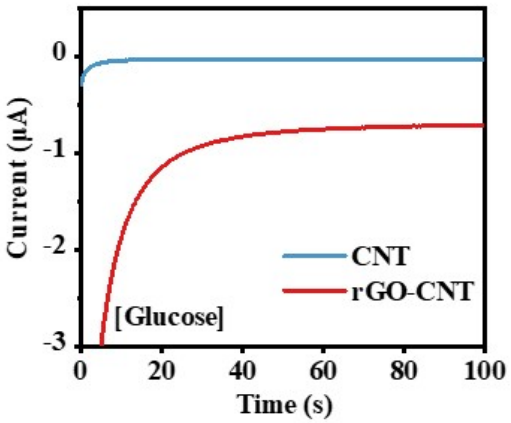

Figure S6. Current curves(i-t) of CNT and rGO-CNT in the same concentration of glucose solution.

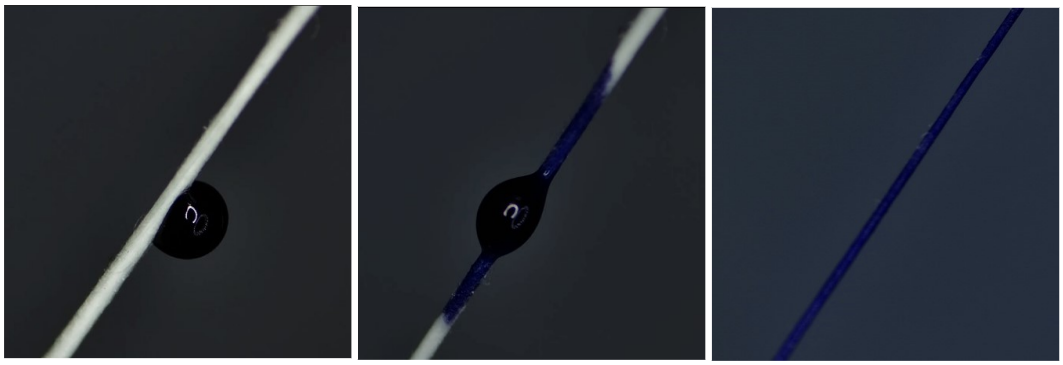

Figure S7. Observation of the ink absorption process on the fiber by optical microscopy.

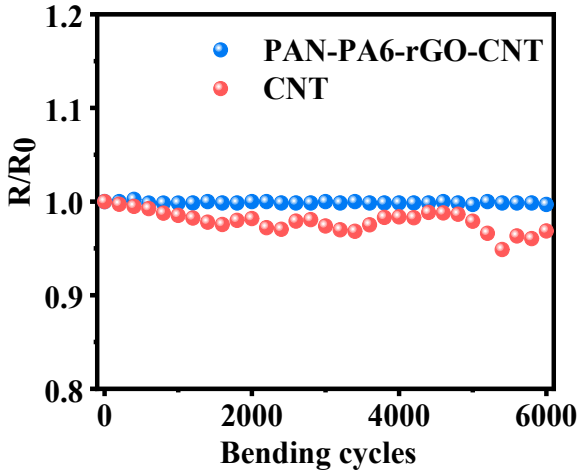

Figure S8. Resistance change of CNT and HFH-ESF after 6000 times of 90 degree bending.

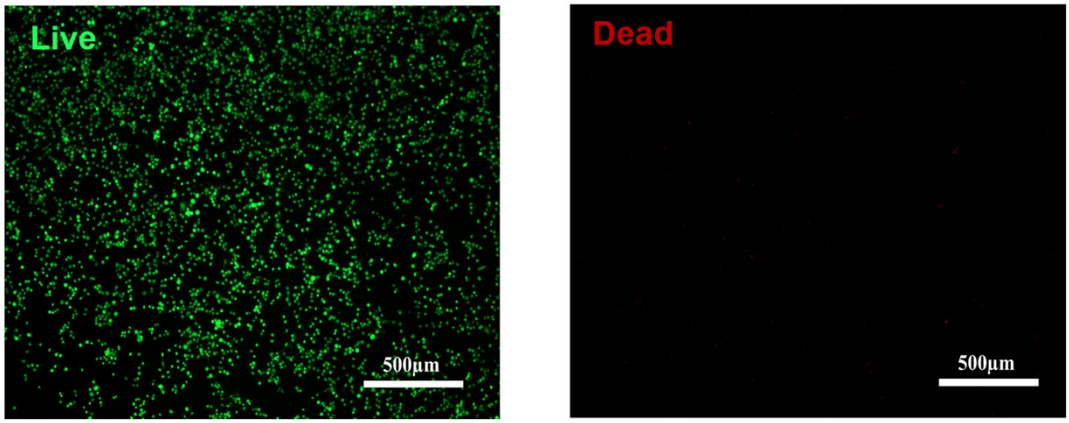

Figure S9. Fluorescent images of live dead cells after 24 hours of cell viability testing in HFH-ESF cultures.

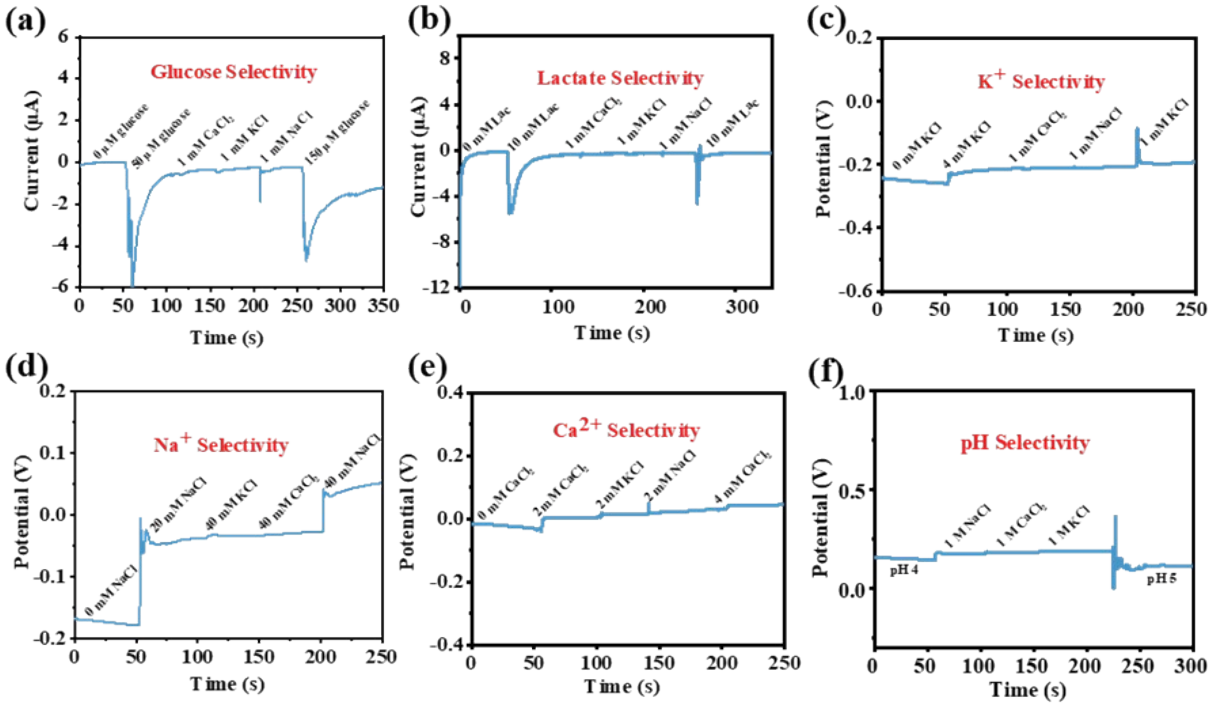

Figure S10. The interference study for individual (a) glucose, (b) lactate, (c) K^+, (d) Na^+, (e) Ca^{2+}, and (f) pH-sensing fibers.

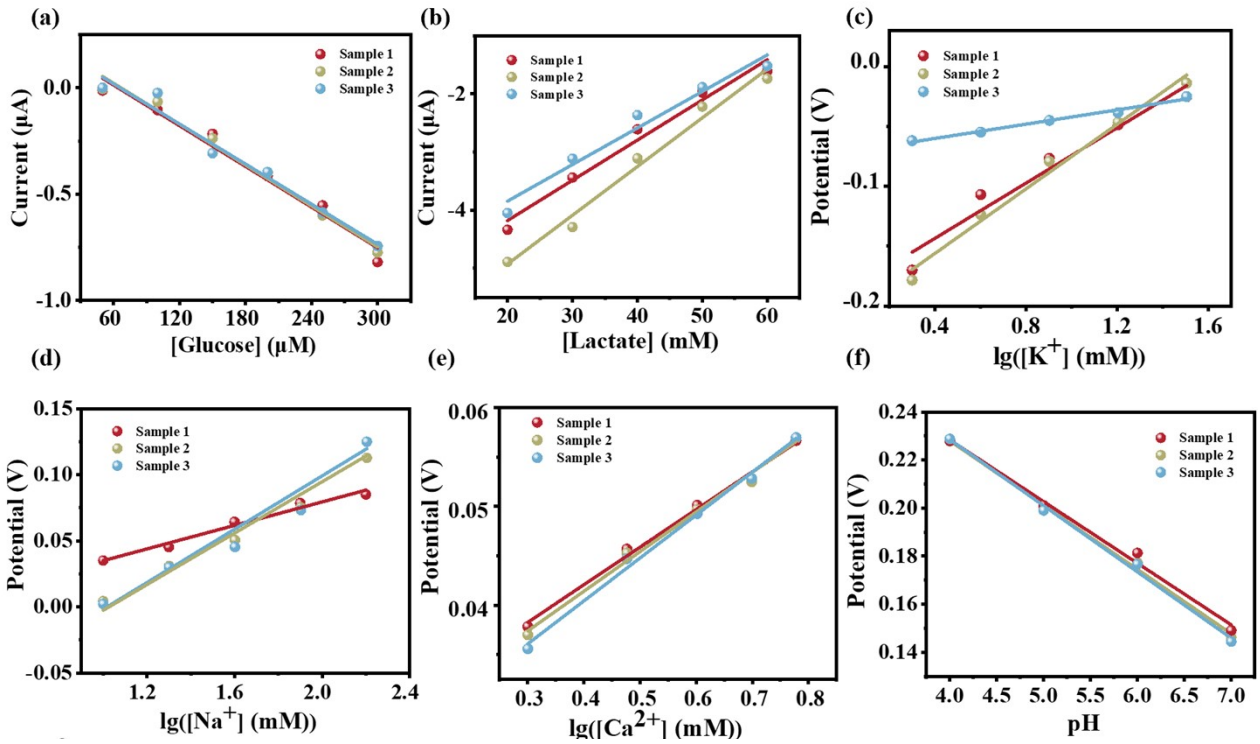

Figure S11. The reproducibility of (a) glucose, (b) lactate, (c) K^+, (d) Na^+, (e) Ca^{2+}, and (f) pH-sensing fibers.

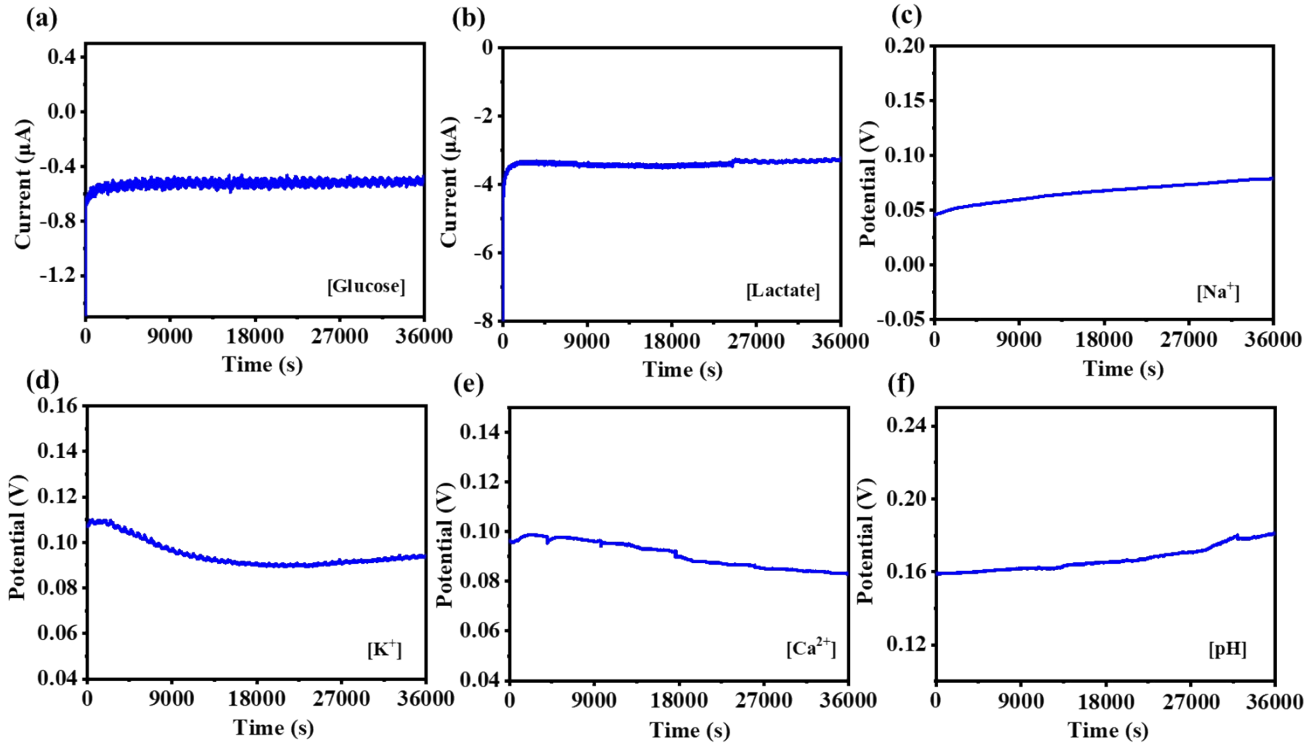

Figure S12. The long-term stability of the (a) glucose, (b) lactate, (c) K^+, (d) Na^+, (e) Ca^{2+}, and (f) pH-sensing fibers Tests were performed in solutions of fixed concentrations. (50 μm glucose, 30 mM lactate, 10 mM NaCl, 4 mM KCl, 6 mM $CaCl_2$, HCl (pH=6))

Figure S13. The processing and structure of textile. (a) Fiber working electrodes and reference electrodes as weft yarns for this work, polyester threads as weft yarns for the other parts of the filling and warp parts. (b) The process and diagram of sewing fabric into clothes